Korean J. Chem. Eng., 38(12), 2381-2396 (2021)
DOI: 10.1007/s11814-021-0896-z

pISSN: 0256-1115
eISSN: 1975-7220

Economic-energy-exergy-risk (3ER) assessment of novel integrated ammonia synthesis process and modified sulfur-iodine cycle for co-production of ammonia and sulfuric acid

JunKyu Park*,†, Junsung Jeon, and Wooyong Um**,***,†**

*Graduate Institute of Ferrous & Energy Materials Technology (GIFT), POSTECH, Pohang 37673, Korea
**Division of Advanced Nuclear Engineering (DANE), Pohang University of Science and Technology (POSTECH), 77 Chongam-ro, Nam-gu, Pohang 37673, Korea
***Division of Environmental Sciences and Engineering (DESE), Pohang University of Science and Technology (POSTECH), 77 Chongam-ro, Nam-gu, Pohang 37673, Korea
(*Received 6 April 2021 • Revised 25 June 2021 • Accepted 7 July 2021*)

Abstract−A novel integrated modified sulfur cycle and ammonia production process was suggested for the co-generation of sulfuric acid. Exergy analysis, heat integration, and safety assessment were conducted to investigate the feasibility and analyze the process. The exergy analysis showed that the highest exergy destruction occurred in the section with the most considerable temperature difference involved with a large flow rate. The heat integration - an economic assessment, confirmed that the total cost was estimated to be reduced by 10.9% at the minimum temperature difference of 39 °C. The failure rate contribution to the overall system was 19%, 11%, 22%, and 47% from the Bunsen section, H_2SO_4 concentration section, HI decomposition section, ammonia production section explosion, fire, and structural damage contributed 82%, 16%, and 2% to the overall system in terms of accident scenario. The accident cost contributed 84% and 16% of accident injury costs to the overall system, respectively. For the sectional based contribution, section 1 (Bunsen process), SA concentration, section 3, and ammonia production process contributed 45%, 29%, 19%, and 6% to the accident injury cost in the overall system, respectively. As a result of individual section failure to the whole section, failure in Bunsen process and HI decomposition led to failure in production of all the products. Failure in NH_3 production section led to production in concentrated H_2SO_4 and H_2. The failure in H_2SO_4 section leads to production in NH_3 and diluted H_2SO_4 concentration. The failure in H_2SO_4 concentration, NH_3 production, and Bunsen process and HI decomposition contributed to the higher failure rate in ascending order.

Keywords: Polygeneration, Sulfuric Acid, Ammonia, Hydrogen, 3ER Analysis

INTRODUCTION

Hydrogen is widely applicable to various areas of fields such as chemical production, energy carriers, and fuel for a mode of transport. The application and production of hydrogen energy has received increasing attention due to high energy density, sustainability, wide application to the chemical industry, environmental benefit, and abundance of raw materials (water) [1]. Sulfuric acid production has been increasing annually since 1950 [2]. Sulfuric acid is widely applicable such as fertilizer, catalyst, alcohols, explosives, drugs, detergents, pharmaceuticals, paper, and petroleum industry [3]. According to sulfur market analysis and forecast report [4], the demand and revenue for the sulfuric acid market were expected to be increasing yearly on USD million scale. Ammonia plays an essential role in the chemical industry with wide application in agricultural products, power cycles, and pesticides. Significantly, ammonia has received increasing attention as a hydrogen carrier and alternative energy storage due to good compressibility, liquefaction at mild conditions (293 K and 0.8 MPa), and high H_2 content [5]. Due to practicality in the modern and future energy carriers, the ammonia market [6] was forecasted to be expanding yearly from 2014-2025 on USD billion scale.

The primary production methods for sulfuric acid are classified into contact process and lead chamber process. For the contact process, the element sulfur is heated with oxygen to produce sulfuric dioxide. Sulfur trioxide is produced by reacting oxygen and sulfur dioxide with the participation of the V_2O_5 catalyst. Then, the sulfuric trioxide is converted to sulfuric acid by reacting with oleum [7]. For the lead chamber process, the sulfur dioxide reacts with each other with oxygen to produce sulfuric trioxide. Then, sulfuric trioxide reacts with water to produce sulfuric acid [8]. The Haber-Bosch process is the most mature technology that produces the majority of ammonia [9]. For the Haber-Bosch process, pressurized hydrogen and nitrogen undergo an equilibrium reaction at 400-500 °C and 250-300 bar to produce ammonia [11]. Nitrogen is obtained from air separation into oxygen and nitrogen, while most hydrogen is extracted from the steam methane reforming [11].

Hydrogen production methods include water electrolysis, liquefied coal, natural gas, and renewable energy source. In the current state, the steam methane reforming process enables large-scale hy-

†To whom correspondence should be addressed.
E-mail: jpark228@postech.ac.kr, wooyongum@postech.ac.kr

drogen production [12]. However, the drawback of steam methane reforming is the mass production of CO_2 greenhouse gas [13]. Thus, the water-splitting process utilizing the renewable-driven is environmentally benign but inefficient due to technological barriers. The thermochemical water-splitting cycle is attractive to be a strong candidate that can enable mass production without carbon dioxide emission [14].

The sulfur-iodine cycle was identified as a promising production method among the thermochemical water-splitting cycle due to its simplicity of operation with a fully fluidized process and high heat efficiency [15]. The sulfur-iodine cycle was initially developed by General Atomics (GA) in the 1970s. This process utilizes high heat (~1,000 °C) from a very-high temperature reactor (VHTR, 4th generation nuclear reaction) with three cyclic reactions (HI decomposition, H_2SO_4 decomposition, Bunsen reaction) using sulfur and iodine compound as a recycling agent in which the net product is oxygen and hydrogen [16]. The process has been extensively investigated to develop the process at the industrial level by the research groups worldwide [17-21]. Excessive iodine is required to maintain good separation in the intermediate process so that researchers carried out experimental work to find the iodine range without pipe clogging [22-28]. Thus, maintaining cyclic reactions of three reactions include additional drawbacks for high temperature, pressure, and corrosive chemicals.

ENEA suggested modifying the sulfur iodine process composed of two reactions: steam as the heat source and SO_2 from flue gas as raw materials. Hydrogen and sulfuric acid, two valuable chemicals, are produced simultaneously. Economic and energy efficiency was determined to evaluate the newly modified sulfur-iodine cycle [29]. A modified sulfur iodine feasibility study was conducted in terms of entropy-based thermodynamics, techno-socio cost, and risk assessment. Furthermore, additional thermodynamic feasibility was investigated with the second law of thermodynamics. A cost and risk comparison analysis between the sulfur iodine cycle and modified sulfur iodine cycle revealed that the failure rate and compensation cost for plant accidents were reduced [30].

Sulfuric acid and ammonia co-production in conventional ways requires three processes that include water-splitting processes such as steam-methane [12] and SI cycle [16], Haber - Bosch process for ammonia production [10], and conventional sulfuric acid processes such as contact process and lead chamber process [8]. However, the integrated modified sulfur iodine cycle [29,30] and Haber-Bosch [9] process produce sulfuric acid and ammonia with only two processes. Such research on polygeneration techniques has been actively engaged in multiple useful chemical and energy production with higher efficiency and fewer processes [31]. Comprehensive diagnosis on sustaining and maintaining such a process is crucial in polygeneration to integrate multiple processes considering safety, heat integration, economic, and thermodynamic feasibility [32].

The main advantage of SI process is high efficiency and low operation cost with fluidized reactions [14]. The disadvantages of the process are material integrity with corrosivity materials (strong acid HI, H_2SO_4, and I_2) and operation maintenance with high temperature three reactions. The advantage of the modified sulfur-iodine cycle is low-temperature, reduced number of reactions, and co-production of hydrogen and sulfuric acid. The possible disadvantages would be emission of harmful gas including NO_X from a steam generator and possibly higher operation cost with steam. Helium or electricity from nuclear reaction is cheaper than medium and high-pressure steam [29,30].

The multi-path safety event tree is a suitable tool to evaluate the multi-integrated event. Fault tree analysis and the event tree analysis are employed for estimating the probability of the accident. The fault tree investigates the hierarchy of events that leads to accidents using the top-down method. The event tree evaluates the success and failure of each accident event [33]. The multi-path event tree exhibits the failure/success of accident events in each unit operator along the pathway so that operators grasp all possible accident pathways in a single figure [34]. Exergy is a quantitative diagnostic method that can measure the thermodynamic efficiency of the target process. Evaluating exergy in each equipment can identify the component required for excessive heat [35]. The heat integration technique exhibits the heat flow through each heating equipment, leading to the minimum heat exchange area, the minimum [36].

This paper suggests a novel two-stage integrated process, Haber-Bosch and modified sulfur iodine cycle, to produce ammonia and sulfuric acid simultaneously. Also, the exergy, energy, an economic assessment was carried out to evaluate the newly developed polygeneration processes for investigating the feasibility.

The following modeling was applied to achieve this research aim: (1) For the first part of process modeling, a modified sulfur iodine cycle (section 2.1.1) was developed based on 1 kmol/h H_2 and 1 kmol/h H_2SO_4. The second part of the modeling (section 2.1.2) was conventional Haber-Bosch for production of 0.6 kmol/h NH_3 with 1 kmol/h H_2 and 0.3 kmol/h N_2 input. (2) Exergy analysis (section 2.2) was carried out on each unit operator to analyze the useful energy in exergy efficiency and destruction. (3) Heat pinch assessment (section 2.3) was utilized to identify the heat flow among heat exchangers. The minimum temperature difference of the heat exchanger network would be identified to search for the optimal cost, which is the trade-off relationship between the capital cost and operating cost. (4) The fault rate of the process and equipment (section 2.4) was analyzed. (5) The economic modeling (section 2.5) was divided into total process cost and accident injury cost. The total process cost (section 2.5.1) includes calculating capital cost (equipment purchase+installation) and operating cost. The accident injury cost (section 2.5.2) includes the cure cost when the injured are exposed to the particular accident scenario.

MATERIALS AND METHOD

The overall scheme for the ammonia and sulfuric acid production system is illustrated in Fig. 1, including external heat source, external feed, and the final products. In this research process, the modified sulfur iodine (MSI) cycle was adopted to produce 1 kmol/h H_2SO_4 and 1 kmol/h H_2, while Haber-Bosch produces 0.6 kmol/h NH_3. Water and SO_2 gas from steam generator were utilized as an external input to the MSI cycle. The steam generator provides external heat both to the ammonia section and modified sulfur iodine cycle. The nitrogen from air separation section is sent to the ammonia section as a reactant, while oxygen is provided to the MSI cycle as a stripping gas. The operating ranges for the MSI cycle

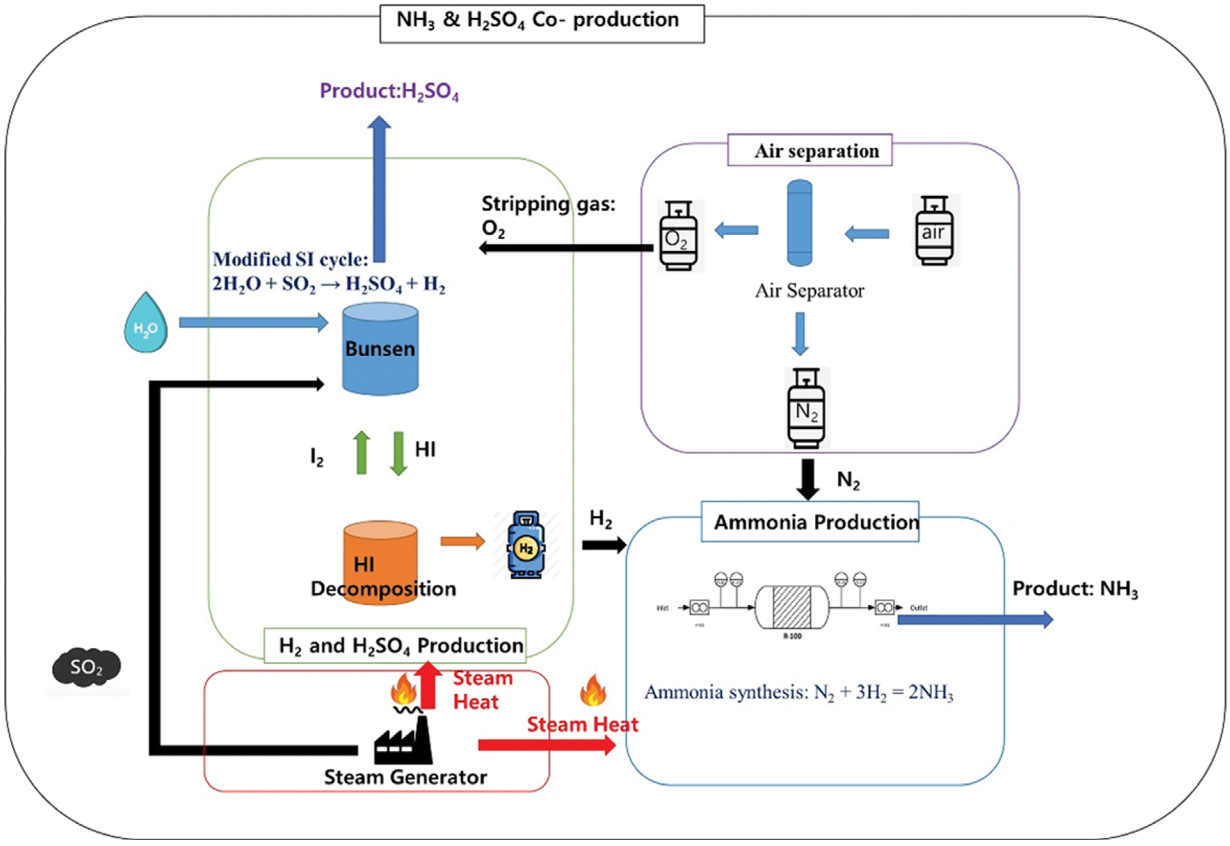

Fig. 1. Integrated modified sulfur-iodine cycle and Haber-Bosch process for co-production of ammonia and sulfuric acid.

and Haber-Bosch were close to each other (450-500 °C).

1. Process Configuration

The process flowsheet for co-production of ammonia and sulfuric acid was constructed using process simulation software. A modified sulfur-iodine cycle flowsheet and Haber-Bosch process were simulated and evaluated using the commercial process simulation software ASPEN PLUS 11.0. The electrolyte non-random two-liquid (ELECNRTL) with Redlich-Kwong (RK) was implemented as the thermodynamic model to implement electrolyte interaction dissociated acid and high pressure, respectively. The recent dataset of HI-H_2O-I_2-H_2 was applied to MSI cycle [37] for better accuracy, which includes the following phase equilibria models: The vapor-liquid equilibrium (VLE) and liquid-liquid equilibrium (LLE) system of HI-H_2O, solid-liquid equilibrium (SLE) for I_2-H_2O, VLE, SLE for HI-I_2, and VLE, and LLE for HI-H_2O-I_2. For the ammonia production section, the Soave-Redlich-Kwong (SRK) was applied to the Haber-Bosch process model [38].

1-1. Modified Sulfur Iodine Cycle

The flowsheet (Fig. 2) of the modified sulfur iodine cycle was constructed to manufacture the co-generation of sulfuric acid (final product) and hydrogen (intermediate product). The high-pressure steam (450-500 °C) from the steam boiler was used as a heat source. The external heat from the steam boiler was only applied to HI decomposition section, which was an endothermic reaction. 1 kmol/h of sulfur dioxide from flue gas and 2 kmol/h water were entering from the external source. The reactions are shown below as indicated in Eqs. (1)-(3):

$$\text{Bunsen process:} \quad I_2+2H_2O+SO_2 \rightarrow 2\,HI+H_2SO_4\ (120\,^{\circ}C) \tag{1}$$

$$\text{HI decomposition:} \quad 2HI \rightarrow H_2+I_2\ (450\,^{\circ}C) \tag{2}$$

$$\text{Net reaction:} \quad 2H_2O+SO_2 \rightarrow H_2SO_4+H_2 \tag{3}$$

In the MSI cycle, Stream 101, a mixture of sulfur dioxide and Section 3 outlet streams, is mixed and reacted with each other in Bunsen reactor (R101). The kinetics information [39] is shown in Eqs. (4)-(5) to denote the production rate of H_2SO_4.

$$r_{Bunsen}=k_1[I_2][H_2O][SO_2] \tag{4}$$

$$k_1=A_1 e^{-\frac{E_1}{RT_1}},\ \text{where } A_1=3\times10^{-6}\ L_2/(mol_2\cdot s) \text{ and } E_1=4.187\ kJ/mol \tag{5}$$

where k_1 is the rate constant for the Bunsen reaction. A_1 is a pre-exponential factor for the Bunsen reaction, E_1 is the activation energy for the Bunsen reaction, and R is the gas constant. The chemical species in the brackets indicate concentration.

Liquid-liquid separation occurs in the decanter unit (S101), in which stream 102 is separated into HI_X with dissolved SO_2 and H_2SO_4 (stream 104) and sulfuric acid solution (stream SA) at 7 bar and 393 K. Oxygen gas (stream 103) from air separator is provided to the bottom of the stripping column (C101), while the HI_X solution (stream 104) enters the top of the stripping column (C101). Oxygen gas (stream 103) is used to strip SO_2 from the HI_X solution

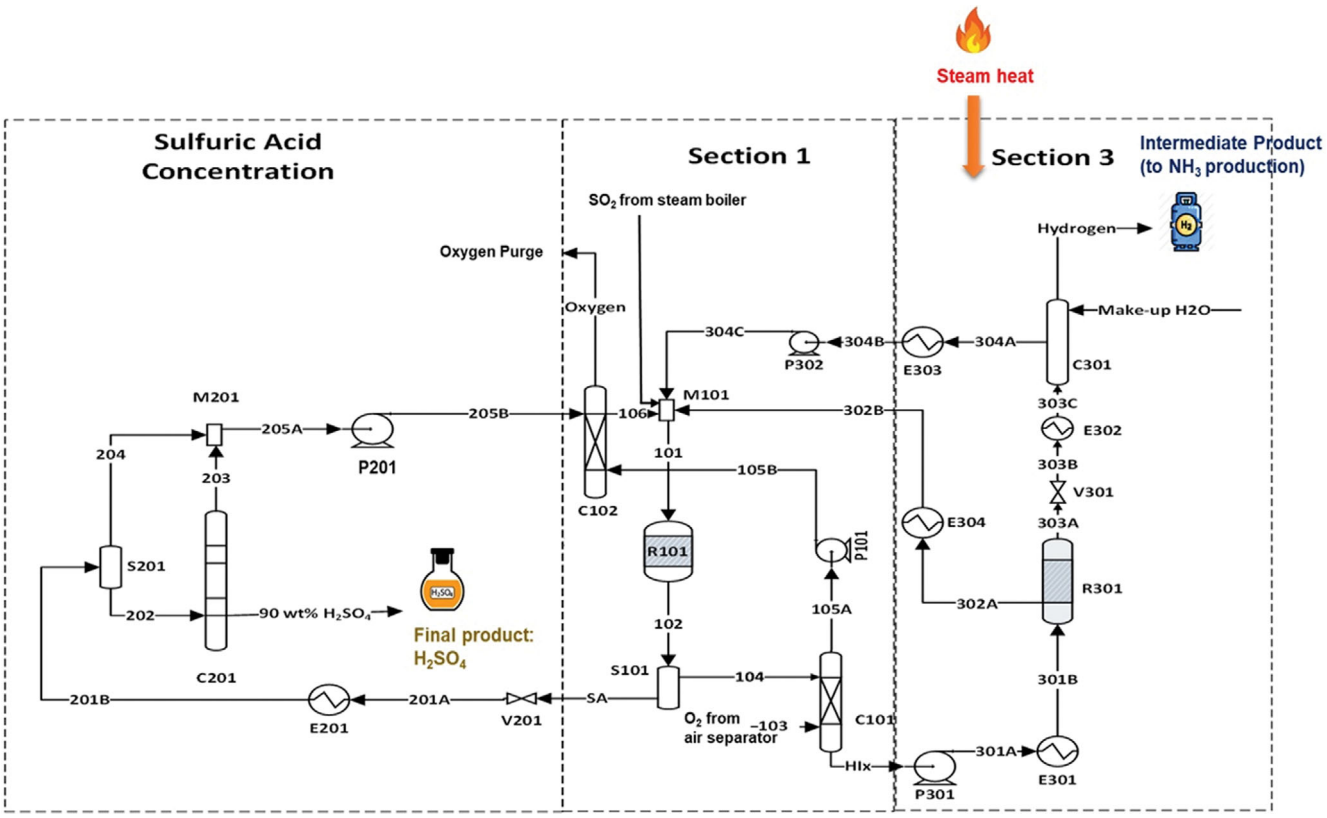

Fig. 2. Production of MSI cycle for 1 kmol/h hydrogen and 1 kmol/h sulfuric acid production to a steam-boiler source.

(stream 104) at 1 bar and 393 K in C101. O_2-SO_2 (stream 105A) gas is vented out of the top of the column at 393 K and 1 bar. The mixture (stream 105A) is pressurized to 10 bar through the pump (P101) and enters the oxygen scrubber (C102). H_2O from section 2 recycle stream (stream 205B) absorbs SO_2 gas from the O_2-SO_2 mixture (stream 105B) at 10 bar and 393 K. The O_2 vents out as purge stream while H_2O-SO_2 solution (stream 106) is recycled back to the Bunsen reactor (R101). The SA stream is sent to the H_2SO_4 concentration unit to produce it as selling-grade sulfuric acid.

SA is heated and depressurized to 1 bar and 424.21 K through a valve (V201) and heat exchanger (201). Then, the H_2SO_4 solution is concentrated to 90 wt% as it is processed through sequential separation in two-phase separation (S201) and a distillation column (C201) at 1 bar. The combined water stream (stream 204, stream 205A) from the top of the sequential separator is fed to an oxygen scrubber (C102) as SO_2 absorbent. The concentrated H_2SO_4 up to 90 wt% purity is sent to the storage tank as a selling product.

The HI_X solution (HI_X) is pre-heated to 723.15 K and pressurized to 10 bar through a preheater (E301) and pump (P301). The treated HI_X solution (stream 301B) enters the reactive distillation column and undergoes a decomposition reaction at 450 °C. A key operation in this column is concurrent reaction and separation. The kinetic equation for HI decomposition considers both forward and reverse reactions as reversible reaction in gas phase. The kinetic reaction information [39] is given in Eqs. (6)-(8):

$$r_{HI}=k_2[HI]^2-k_{-2}[H_2][I_2] \quad (6)$$

$$k_2=A_2e^{-\frac{E_2}{RT_2}} \quad (7)$$

$$k_{-2}=A_{-2}e^{-\frac{E_{-2}}{RT_2}} \quad (8)$$

A_2=1,011 L/(mol·s), E_2=184 kJ/mol

A_{-2}=1.596×107 L/(mol·s), E_{-2}=108 kJ/mol

where k_2 is the rate constant for the forward reaction in HI decomposition, A_2 is a pre-exponential factor for the forward reaction in HI decomposition, and E_2 is the activation energy for the forward reaction in HI decomposition. k_{-2} is a rate constant for the reverse reaction in HI decomposition, A_{-2} is a pre-exponential factor for the reverse reaction in HI decomposition, and E_{-2} is the activation energy for the reverse reaction in HI decomposition. R is the gas constant. Again, the brackets indicate concentration.

1-2. Ammonia Synthesis Process

Streams of 1 kmol/h hydrogen from MSI cycle and 0.3 kmol/h N_2 from air separation units enter the ammonia production section as shown in Fig. 3 [39]. The hydrogen stream (H_2 supply) from C301 is heated to 553.15 K. The mixed stream (401) of nitrogen gas (N_2 supply) and hydrogen gas is compressed to 151 bar at the compressor (C401). The pressurized gas (402) is preheated to 755 K (E401) and enters the reaction chamber (R401). The Haber-Bosch reaction [39] occurs at 755 K and 150 bar, as shown in Eq. (9). The reaction is governed by equilibrium with pressure, as shown in Eq. (10).

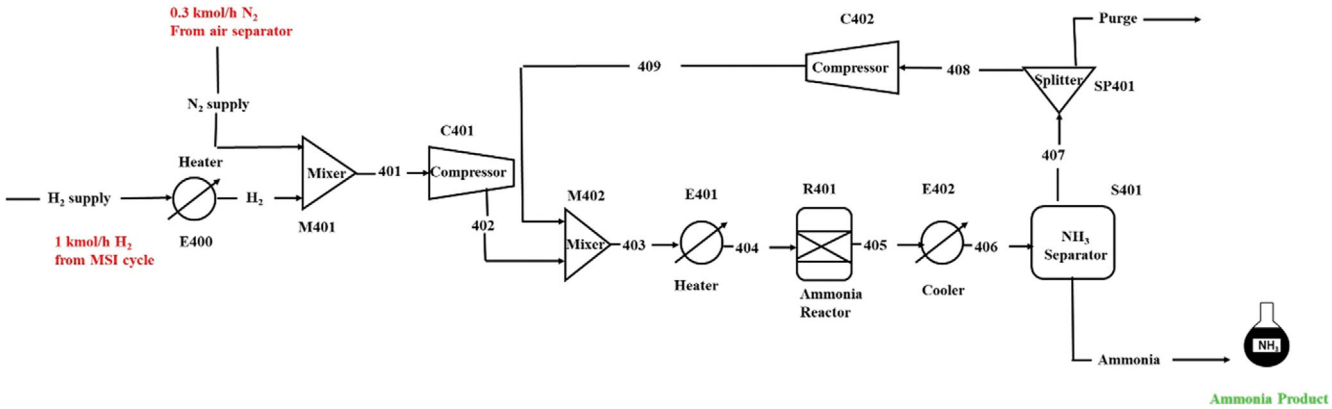

Fig. 3. Ammonia production (0.6 kmol/h) flowsheet with hydrogen and nitrogen feed implementing conventional Haber-Bosch process.

$$N_2+3H_2\leftrightarrow 2NH_3 \tag{9}$$

$$K=\frac{y_{NH_3}^2}{y_{N_2}y_{H_2}^3}\left(\frac{P_0}{P}\right)^2 \tag{10}$$

where K is the equilibrium constant, y_{NH_3} is the mole fraction of ammonia, y_{N_2} is the mole fraction of nitrogen, and y_{H_2} is the mole fraction of hydrogen. P_0 is atmospheric pressure, and P is the operating pressure in the reactor.

In the NH_3 separator (S401), the liquefied ammonia (Ammonia stream) is sent to storage as a selling product, while the unreacted hydrogen and nitrogen (407) recycle back to the mixer (M402). 1% of unreacted nitrogen and hydrogen (stream purge) was purged out of the system.

2. Exergy Evaluation on Thermodynamics

Exergy is the quantitative value representing the maximum useful energy when the system is assumed to be in equilibrium with the environment [40]. The advantage of exergy is that it is practical to provide the guideline to judge the efficient and inefficient components in the thermodynamic analysis. Exergy analysis in a modified cycle aims to identify the unit operator that requires an external energy source. The exergy analysis has been carried out in the sulfur-iodine cycle based on solar energy sources in previous researches [41].

The exergy balance equation is classified into chemical and physical exergy. The physical exergy represents the maximum useful energy in mechanical and physical unit operator such as heat, mix, and pressure change. The chemical exergy is exerted to the chemical process system such as chemical separation (e.g., absorption, distillation) and reaction. The exergy balance equation can be derived by combining the first and second laws of thermodynamics shown in Eqs. (11)-(12):

$$\Sigma EX_{in}+Q\left(1-\frac{T_0}{T}\right)=\Sigma EX_{out}+EX_W+EX_D \tag{11}$$

$$EX=Q\left(1-\frac{T_0}{T}\right) \tag{12}$$

where EX_{in} and EX_{out} are, respectively, inlets and outlet exergy of the control volume. Q, T, T_0 are the amount of heat transferred, operating temperature, and reference environment temperature. EX_W and EX_D represent the exergy of work and the exergy of destruction due to irreversibility, respectively.

EX_{in} and EX_{out} can be divided into the physical exergy and chemical exergy [42] as the following Eqs. (13)-(14):

$$EX=EX_{PH}+EX_{CH} \tag{13}$$

$$EX=(H-H_0)+T_0(S-S_0)+EX_{CH} \tag{14}$$

where EX_{PH} and EX_{CH} are the physical exergy and chemical exergy, respectively. H and H_0 are the enthalpy and enthalpy at reference state, respectively. S and S_0 are the entropy and entropy at the reference state. T_0 is the temperature at the reference state.

The exergy destruction and the exergy efficiency of the unit operator can be calculated by the following as shown in Eqs. (15)-(16):

$$EX_D=EX_{in}-EX_{out}+EX_Q-EX_W \tag{15}$$

$$\eta_{EX}=1-\frac{EX_D}{EX_{in}} \tag{16}$$

where η_{EX} represents exergy efficiency. EX_D is exergy of destruction.

3. Heat Pinch Integration for Capital and Operating Cost Optimization

Heat integration is an essential factor in efficiently managing the polygeneration process. In this study, heat pinch integration was conducted using ASPEN PLUS Energy Analyzer V11. The scope of heat integration was to identify the optimal minimum heat pinch temperature, which considers the trade-off between capital cost and operating cost. In previous studies, heat integration had not been investigated in the modified sulfur-iodine cycle. The heat integration was carried out to investigate the configuration of heat flow and the minimum pinch point. Steam and cooling water were considered as external utility systems. The heat pinch assessment provides a visual aid to make it easy to understand the connection between heat exchangers [43]. The first step is to identify the hot stream that transfers heat to the cold stream, and temperature drop occurs while the cold stream where transfers heat to the cold stream and temperature rise occurs [43].

The heat transfer amount for each heat exchanger should be identified as the second step of heat integration [34]. The heat transfer equation for the heat exchanger is shown in Eq. (17).

$$Q=UA\cdot LMTD \quad (17)$$

where Q is the amount of heat transferred from the heat exchanger. U is the overall heat transfer coefficient. A is the heat transfer area. LMTD is the logarithmic mean temperature difference for driving force temperature.

The overall heat transfer coefficient is determined from the fluid and heat transfer coefficient. Overall heat transfer coefficient is composed of heat conduction and heat convection. The required fluid and metal properties such as heat capacity, thermal conductivity, viscosity, and molar density are transferred from properties data in ASPEN PLUS simulation.

4. Risk Assessment on the Integrated Ammonia and Modified Sulfur-iodine Cycle

The accident probability was investigated to integrate ammonia and modified sulfur iodine cycle based on fault tree analysis [30]. Fault tree assessment is a simple but powerful technique to investigate the probability of an accident. As indicated in Fig. 4, each basic event in a blue box indicates the accident event, such as fire, explosion, and structural damage. The intermediate event, in this case, represents each equipment. The augment of basic event contributes to the intermediate event. The sum of the intermediate events contributes to the total event. The total event indicates the failure probability of ammonia and sulfuric acid production. The equipment failure probability extracted from OREDA database [48] was employed to reflect the off-shore equipment in the plant. The comprehensive FTA technique (Fig. 4) was employed to evaluate the failure accident event, such as fire, explosion, and structure damage to equipment [50]. This study assumed that failure in any equipment (OR) gate would cause the halt system to observe the maximum probability of failure.

The failure rate for each equipment in section 1, sulfuric acid concentration, section 3, and ammonia product sector is represented with the bar graph. The percentage of accident rate and each section to the overall system was analyzed in order to investigate the contribution of each component. The accident event for each type of equipment (e.g., reactor, column, and vessel) is also provided in the result section. The failure rate was implemented in the accident injury cost, which is a quantitative representation of injury in terms of cost.

The failure rate investigation via fault tree technique gives an insight into distribution and proportion according to accident type and each section (section 1, section 3, NH_3 production). However, fault tree analysis is limited in that it only shows the total failure and individual components. To resolve that issue, the partial failure by one of the sections has been investigated as shown in the following section.

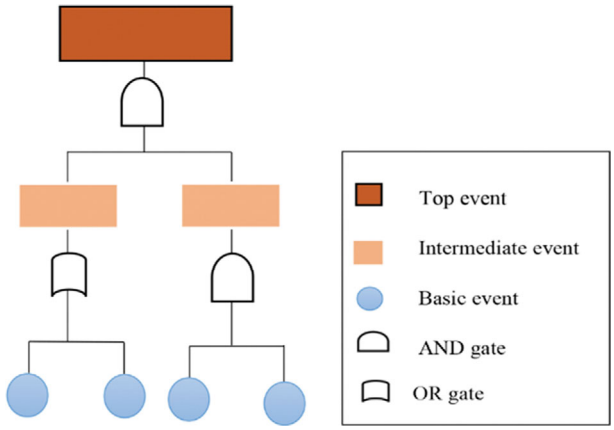

Fig. 4. Schematic diagram of fault tree components.

(a) Bunsen process failure
(b) HI decomposition failure
(c) NH_3 production failure
(d) H_2SO_4 concentration failure

The aforementioned partial failure cases (a)-(d) are implemented to Fig. 5. As a result, the failure rate of each case, availability of product, and neighboring effect is investigated and discussed. The total failure shown in Fig. 5 indicates the total failure of each section based on fault tree analysis. The failure rate of partial failure is calculated by OR gate logics, which means the sum of the probability. This notion is because the failure in one sector leads to the total failure in next sector rather than failure in two events leading to total failure. For instance, If HI decomposition has malfunctioned, hydrogen cannot be provided to NH_3 production section. Chain of events would be expected to occur if the operation in one section stopped.

5. Economic Modeling

The economic modeling in this section is divided in techno-

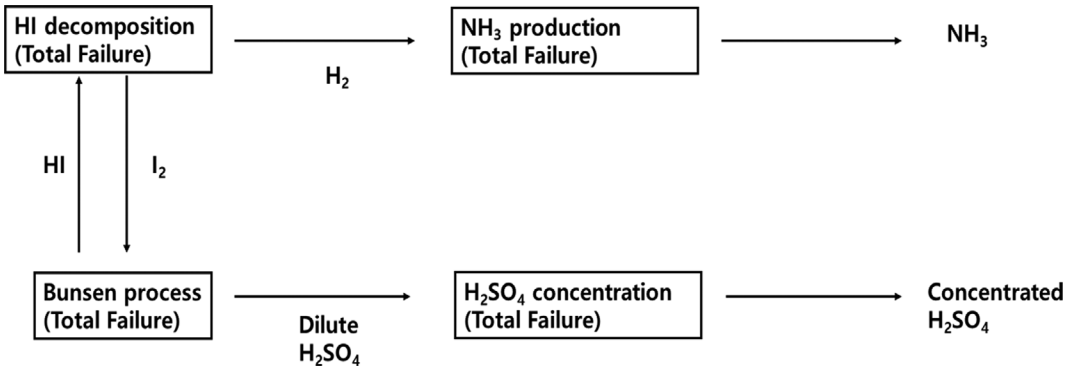

Fig. 5. Schematic for investigating neighboring sector.

Table 1. Purchase cost coefficients, pressure coefficients, and sizing/capacity of A for equipment types in purchase cost equations [46]

Equipment type	K_1	K_2	K_3	C_1	C_2	C_3	A
Centrifugal pump	3.3892	0.0536	0.1538	−0.3935	0.3957	−0.00226	Power (kW)
Compressor	2.2891	1.3604	−0.1027	−0.2454	0.2590	−0.0136	Power (kW)
Heat exchanger	4.3247	−0.303	0.1634	−0.00164	−0.00627	0.0123	Heat transfer area (m^2)
Vertical vessel	3.4974	0.4485	0.1074	$\frac{(P+1)D}{2*[850-0.6(P+1)]}+0.00315$			Diameter (m), height (m)
Horizontal vessel	3.5565	0.3776	0.0905	0.0063			Diameter (m), length (m)

economic modeling (2.5.1) and accident injury cost (2.5.2). The techno-economic cost is used in heat integration to optimize the total cost by investigating operation cost and capital cost. For safety, accident injury cost is utilized to quantify the accident in terms of cost.

5-1. Techno-economic Modeling

The operating cost and capital cost were calculated for the modified sulfur iodine cycle and ammonia production plant. The air separation unit was excluded from the economic cost assessment. The components in chemical cost are the cost required for the initial setup of the plants such as purchased equipment cost, the installation cost for equipment and auxiliary (piping and electricity), land cost, contingency [43]. Operating cost considers the cost required for operating a plant, such as utility, catalysts, raw materials, labor, and maintenance [46].

The bare module technique was implemented for evaluating the capital cost of the equipment. The purchased cost calculation of the equipment was required for total capital calculation. The purchased equipment was considered as the basis of the capital cost calculation. The purchase cost of equipment was calculated using a bare module costing method, as shown in Eq. (18):

$$C_{PEC}=f_m \cdot f_p \cdot C^0_{PEC} \tag{18}$$

where C_{PEC} is the purchase cost of the equipment, f_m is the material factor. f_p is the pressure factor, and C^0_{PEC} is the purchase cost of the equipment at ambient temperature and pressure.

The purchase cost of the equipment at atmospheric pressure (C^0_{PEC}) was estimated using Eq. (19).

$$\log_{10}C^0_{PEC}=K_1+K_2 \log_{10}A+K_3 (\log_{10}A)^2 \tag{19}$$

where K_1, K_2, and K_3 are constants of purchase equipment cost at atmospheric pressure, and A is equipment capacity or size.

K_1, K_2, and K_3 were determined by the type of equipment (e.g., pump, heat exchanger). The equipment capacity factor (A) was obtained from the process simulation result. The pressure factor (f_p) was calculated as a correction factor for atmospheric pressure using Eq. (20):

$$\log_{10}f_p=C_1+C_2 \log_{10}P+C_3 (\log_{10}P)^2 \tag{20}$$

where C_1, C_2, C_3 are constants for pressure factor, and P is the operating pressure.

The type of equipment determined constants for pressure factors (C_1, C_2, C_3). Also, operating pressure (P) was obtained from the input operating pressure for process simulation. The factors required for purchased equipment cost, such as the purchased equipment coefficients (K_1, K_2, and K_3), equipment capacity or sizing (A), and pressure factor coefficients (C_1, C_2, and C_3), are summarized in Table 1 [46].

Table 2. Total capital cost estimation based on a fraction of the delivered equipment cost method in a fluid processing plant [46]

Components	Fraction of PEC
Direct cost (C_D)	
Purchased equipment cost	1.00
Delivery	0.10
Purchased equipment installation	0.47
Instrumentation and control	0.36
Piping	0.68
Electrical system	0.11
Building	0.18
Yard improvements	0.10
Service facility	0.70
Indirect cost (C_{ID})	
Engineering and supervision	0.33
Construction expense	0.41
Legal expense	0.04
Contractor's fee	0.22
Contingency	0.44

The total capital cost was evaluated using the purchase cost of equipment, as shown in Eq. (21) and Table 1 [26]. The factors for each component as shown in Table 2 are those for a fully fluidized process in a chemical plant. Direct cost (C_D) and indirect cost (C_{ID}) were obtained by multiplying each factor by the equipment purchase cost. The sum of C_{PEC} values (from Eq. (18)) and C_D and C_{ID} from the multiplication of C_{PEC} values resulted in total capital cost as represented in Eq. (21).

$$TCC=C_{PEC}+C_D+C_{ID} \tag{21}$$

where C_{PEC} is the purchase cost of equipment, C_D is direct cost, C_{ID} is an indirect cost, and TCC is the total capital cost.

The operation cost includes the cost required for the maintenance and operation of the process. The operation cost was calculated using Eq. (22) and (23). The utility of the modified sulfur iodine cycle and ammonia production section consists of low-pressure steam, high-pressure steam, cooling water, and electricity as shown in Eq. (22).

Table 3. Treatment costs of injuries as a consequence of accidents according to piece of equipment [47]

Accident (subscript j)	Injuries (subscript i)	Cure cost (C_{ei})
Fire	Toxic exposure (CO gas)	\$133/year·person
	Burn	\$125/year·person
Explosion	Blast lung	\$433/year·person
	Bone fracture	\$141/year·person
Inhalation of NO_x	Breathing impairment	\$121/year·person

$$TOC=C_U+C_{raw}+C_{cat}+C_{main} \quad (22)$$

$$C_U=C_{CW}+C_E+C_{HP}+C_{LP} \quad (23)$$

where TOC is total operating cost, C_U is utility cost, C_{raw} is raw materials such as inlet chemicals consumed, C_{cat} is the cost of catalyst, and C_{main} is the maintenance cost. C_{CW} is the cost for cooling water, C_E is the cost for electricity, C_{HP} is the cost for high-pressure steam for a steam boiler, and C_{LP} is the cost for low-pressure steam.

5-2. Accident Injury Cost for Accident Occurrence Scenario

The accident injury cost assessment provides a quantitative way to evaluate the accident in terms of cost. For the modified sulfur iodine cycle, accidents from a chemical plant and toxic gas dispersion (NO_X) pose possible health risks. The accident for ammonia production section includes explosion from hydrogen and high pressure operation. The accident injury cost assessment was evaluated for a population of 200,000 in a virtual city near the plant. The accident injury cost was calculated by the cost of the number of people exposed to the different types of accidents.

The total number of people multiplied by accident probability for each accident resulted in the number of people affected by the particular accident implementing Eq. (26). The failure rate for each piece of equipment was identified from the multi-path safety assessment. The accident injury cost was calculated by multiplying the number of people exposed to accidents by the cure cost required for each accident (Table 3). The accident injury cost of each equipment is calculated by multiplying the number of people injured and the cost of treatment cost related to the type of injury. Finally, the sum of all cure costs related to all accidents in all equipment types is the total cure cost as shown in Eq. (27).

$$N_i=f_j \text{ X } N_T \quad (26)$$

$$SHC=\Sigma_{i=1}^{n}(N_i \text{ X } C_{ci}) \quad (27)$$

where SHC is the accident injury cost, N_i is the total number of people exposed to injuries i from accident j, C_{ci} is the treatment cost to cure injury of accident j, f_j is the failure rate of each piece of equipment in accident j, and N_T is the total number of residents in the virtual area.

RESULTS AND DISCUSSION

1. Exergy Analysis

The exergy of unit operators in the modified sulfur-iodine cycle and ammonia production was investigating the useful energy in each section. The exergy destruction and exergy efficiency are illustrated in Fig. 6 along the exergy destruction distribution in terms of section and equipment.

The exergy destruction in section 1 was distributed to be 14.06 kW, 9.99 kW, 6.5 kW, 1.59 kW, 0.71 kW, and 0.49 kW allocated to the unit operators Bunsen reactor (R101), liquid-gas separation drum (S101), stripping column (C101), absorption column (C102), heat exchanger (E101), and pump (P101) according to Fig. 6(a). The R101, S101, and C101 showed relatively higher exergy destruction compared to the other unit operators. The exergy destruction of C102, E101, and P101 showed a low exergy value less than 2.00 kW. Among them, P101 presents the lowest quantities of destructive exergy. The high exergy destruction was observed for R101, S101, and C101 because the loss resulted from heat exergy change for reaction and chemical exergy change separation process from the combined flow from unit M101. On the other hand, C101 revealed the lowest among R101, S101, and C101 because the lower flow rate was involved in which H_2SO_4 solution stream was separated in S101.

The contribution of exergy destruction in section 2 was 10.38 kW, 2.59 kW. 1.92 kW, and 0.000644 kW allocated to E201, C201, P201, and P201 as shown in Fig. 6(a). E201 and C201 showed higher exergy destruction due to the heating. The heating was involved in the reboiler column attached to the distillation column. S201 showed the third highest exergy destruction due to loss from chemical separation.

For section 3, the exergy destruction contributions to the system were 127.24 kW, 21.24 kW, 2.06 kW, 98.99 kW, 1.61 kW, and 39.82 kW, respectively, from the heat exchanger (E301), a heat exchanger (E302), a heat exchanger (E303), heat exchanger (E304), H_2 wash column (C301), and HI decomposition reactor (R301) as indicated in Fig. 6(a). The exergy destruction was arranged to C301, E303, E302, R301, E304, and E301 in ascending order. The high exergy destruction was exhibited in heat exchangers (E301, E304) due to temperature change with a high flow rate. HI decomposition reactor (R301) presents the third-highest exergy destruction due to loss from high temperature and endothermic heat of reaction. The fourth highest exergy destruction occurred in E303 due to cooling in the vapor phase. The C301 and E302 occupied the lowest exergy destruction due to mere cooling with a small flow rate in C301 unit and a low flow rate with low temperature change in heating for E303 unit.

The exergy destruction in ammonia section was distributed to be 2.15 kW, 18.16 kW, 21.42 kW, 7.29 kW, 10.03 kW, 2.9 kW, and 1.21 kW allocated to E400, E401, E402, C401, C402, R401, and S401 as illustrated in Fig. 5(a). After the preheating, the heating units and compressors exhibited exergy destruction above 7 kW in

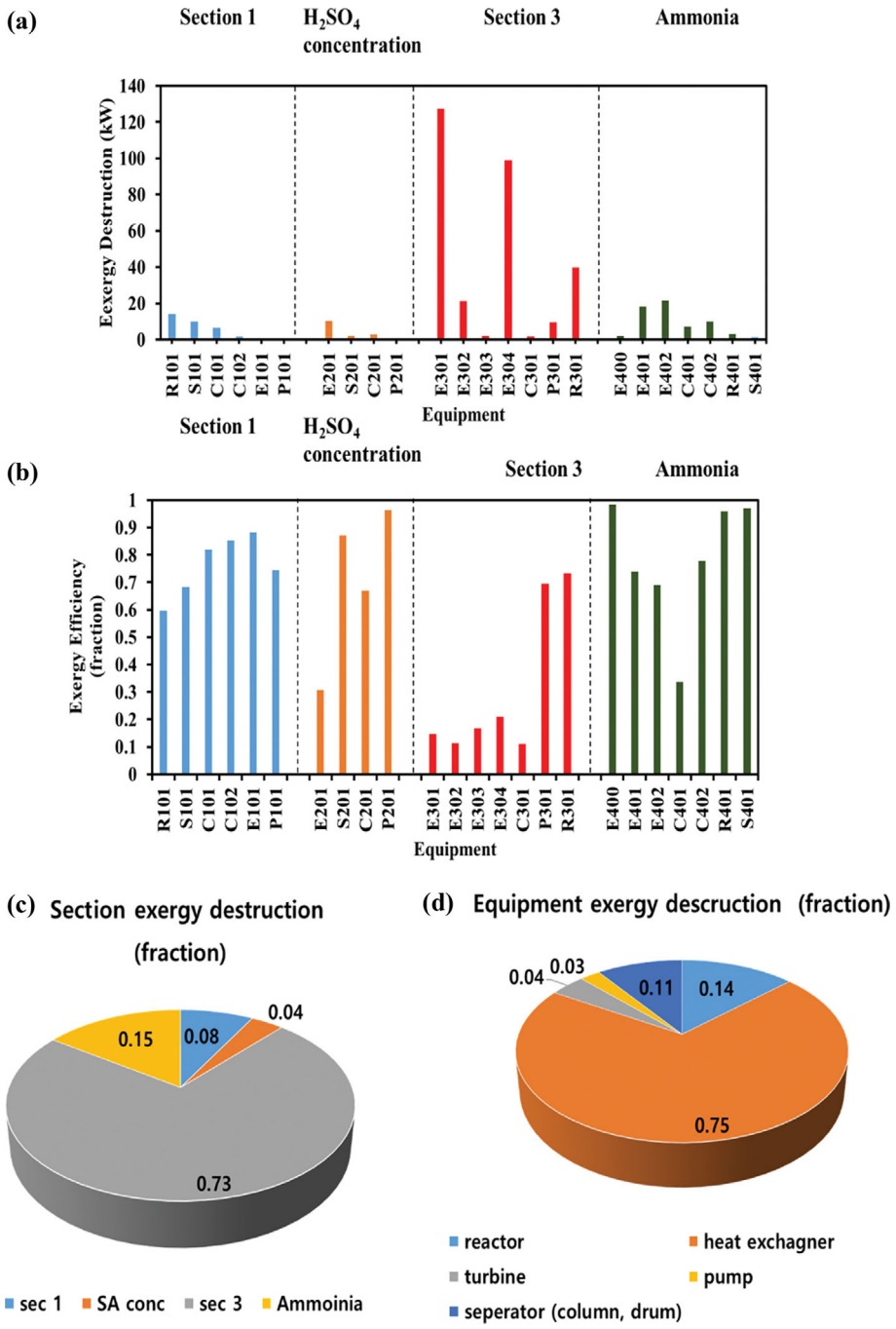

Fig. 6. Exergy analysis on modified sulfur iodine cycle. SA conc. indicates sulfuric acid concentration (a) exergy destruction, (b) exergy efficiency, (c) exergy destruction distribution for sections, (d) exergy destruction distribution for equipment.

which unit operators were E401, E402, C401, and C402. The cooling after the reactor (E402) and heating unit (E401) after the reactor exhibited the highest exergy destruction where the large temperature change occurred. The pre-heating section (E400) and ammonia production reactor (R401) contributed to the second largest group with exergy destruction value. The simple two-phase separator, S101, revealed the lowest exergy destruction.

The exergy efficiency for all the unit operations in each section is illustrated in Fig. 6(b). In general, the exergy efficiency of unit operators in section 3 was revealed to be the lowest among the group. Especially, heat exchanger units (E401, E402, E403, and E404) showed low exergy efficiency among all the unit operators. The exergy efficiency in section 1 exhibited relatively high exergy efficiency, falling in the range of 0.5-0.8. However, the unit operators in section 1 did not exceed exergy efficiency to 0.9 because large flow rate was involved with the combined stream from H_2SO_4 concentration and section 3. The H_2SO_4 concentration section and ammonia production exhibited a fluctuating exergy efficiency dis-

tribution because of the small flowrate with a higher temperature than section 1.

The exergy destruction distribution is shown in Fig. 6(c) and (d). Sulfuric acid concentration, section 1, ammonia production, and section 3 were contributing 4%, 8%, 73%, and 15% in ascending order as illustrated in Fig. 6(c). The heat exchanger, reactor, separator, turbine, pump were distributed to 75%, 14%, 11%, 4%, and 3% in descending order. To sum up, the section with high temperature and large flow rate exhibited low exergy efficiency and high exergy destruction. The opposite trend was revealed for lower temperature and lower flow rate.

2. Economic and Heat Assessment for Determining Minimum Temperature Difference

The integrated heat pinch and economic assessment was performed to minimize the total cost. The variation of the total cost, capital cost, and operating cost is illustrated in Fig. 7 by varying the minimum heat temperature difference. According to economic assessment, the capital cost and operation cost of combined modified sulfur iodine cycle and ammonia production processes were \$16.24 million and \$56,009 with the minimum temperature difference of 10 °C. The capital cost and operating cost were \$11.45 million and \$39,892 for the modified sulfur iodine cycle [30]. For the ammonia production section, the capital and operating cost was \$4.79 million and \$16,117, respectively.

The leverage between the capital cost and operating cost is illustrated in Fig. 7(a) with the minimum temperature difference change. The capital cost decreases in a logarithmic pattern from \$2.0293 million to \$1.296 million as the minimum temperature difference changes from 1 °C to 50 °C. In contrast, the operating cost exhibits its semi-linear growth from $\$4.128\times10^4$ to $\$2.147\times10^5$ in the minimum temperature range from 1 °C to 50 °C. The capital cost and operating cost show the inverse trend as the increase in the minimum temperature difference. The heat exchanger required a larger area (increase in capital cost) to maintain heat transfer for a smaller minimum temperature difference; the required utility (decrease in operating cost) decreased with a smaller minimum temperature difference. For the higher temperature difference, the notion was quite the opposite that smaller heat exchange area (decrease in capital cost) and more utility were required (increase in operating cost).

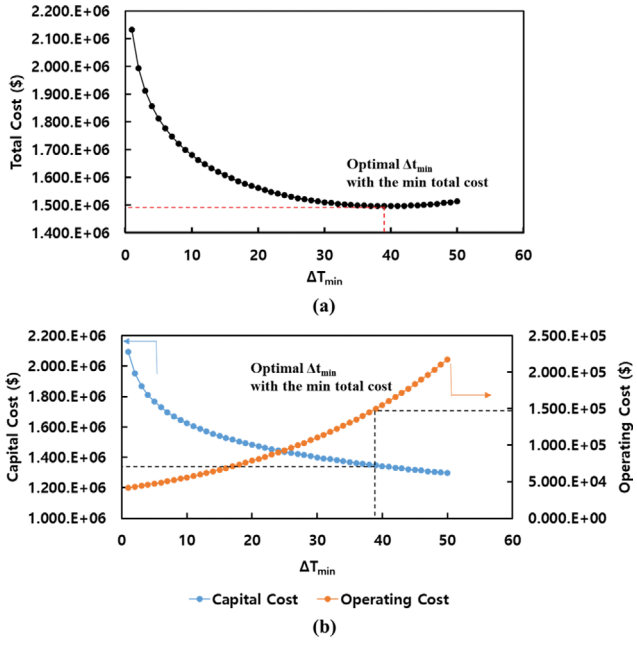

Fig. 7. Variation of cost according to minimum temperature (ΔT_{min}) of ammonia and modified sulfur iodine cycle (a) operating and capital cost, (b) total cost for determining the ideal minimum temperature difference.

Fig. 7(b) illustrates the total cost variation (operating cost+capital cost) with the minimum temperature difference. From that graph, the minimum total cost and minimum temperature difference were extracted. The total cost exhibits an exponential reduction along with the minimum temperature difference. From 1 °C to 30 °C, the total cost reveals the exponential decrease from \$2.134 million to \$1.511 million. The total cost exhibits a slight decrease from \$1.508 million to \$1.497 million with a temperature range of 30 °C to 39 °C. The total cost increased gradually from \$1.498 million to \$1.514 million when the minimum temperature increased from 30 °C to 50 °C. Therefore, the optimal minimum temperature was 39 °C with the minimum total cost of \$1.497 million with a capital cost of \$1.347 million and an operating cost of $\$1.447\times10^5$. That indicates 10.9% (minimum temperature difference: 39 °C) cost saving compared to the design basis case with the minimum temperature of 10 °C.

3. Risk Assessment Integrated MSI and Ammonia Production Process

The failure rate of each equipment and each accident scenario is demonstrated as shown in Fig. 8 and Table 4. The accident scenario of the reactor, column, vessel drum, pump, and the turbine was generated based on HAZOP study [30]. The failure probability per each type of equipment was obtained from OREDA database [48], and a chemical safety literature review [49] was used to allocate the probability of each accident scenario.

Pump (P101), heat exchanger (E101), stripping column (C101), absorption column (C102), flash vessel (R101), and Bunsen reactor (S101) were contributing to failure in section 1 in ascending order. In general, the reactor required the heating section to maintain the reaction. The columns were contributing to the second largest failure rate due to pressure operation with complicated structure. The ascending order of failure rate is a pump (P201), a heat exchanger (E201), distillation column (C201), and flash drum (S201) contributing to the H_2SO_4 concentration section in ascending order. Pump (P301), a heat exchanger (E301, E302, E303, E304), wash column (C301), and reactor (R301) contributed to the failure rate in increasing order. For the ammonia process section, heat exchangers (E400, E401, E402), flash drum (S401), and compressors (C401 and C402) contributed to the ammonia production sector in increasing order.

To sum up, the failure rate contributions to the overall system were 19%, 11%, 22%, and 47% from the Bunsen section, H_2SO_4 concentration section, HI decomposition section, ammonia production section, respectively. Ammonia exhibited the highest risk because of high pressure operation with hydrogen gas. Section 2 exhibited the lowest risk due to the smallest number of equipment operating. Section 3 exhibited the second largest portion of the

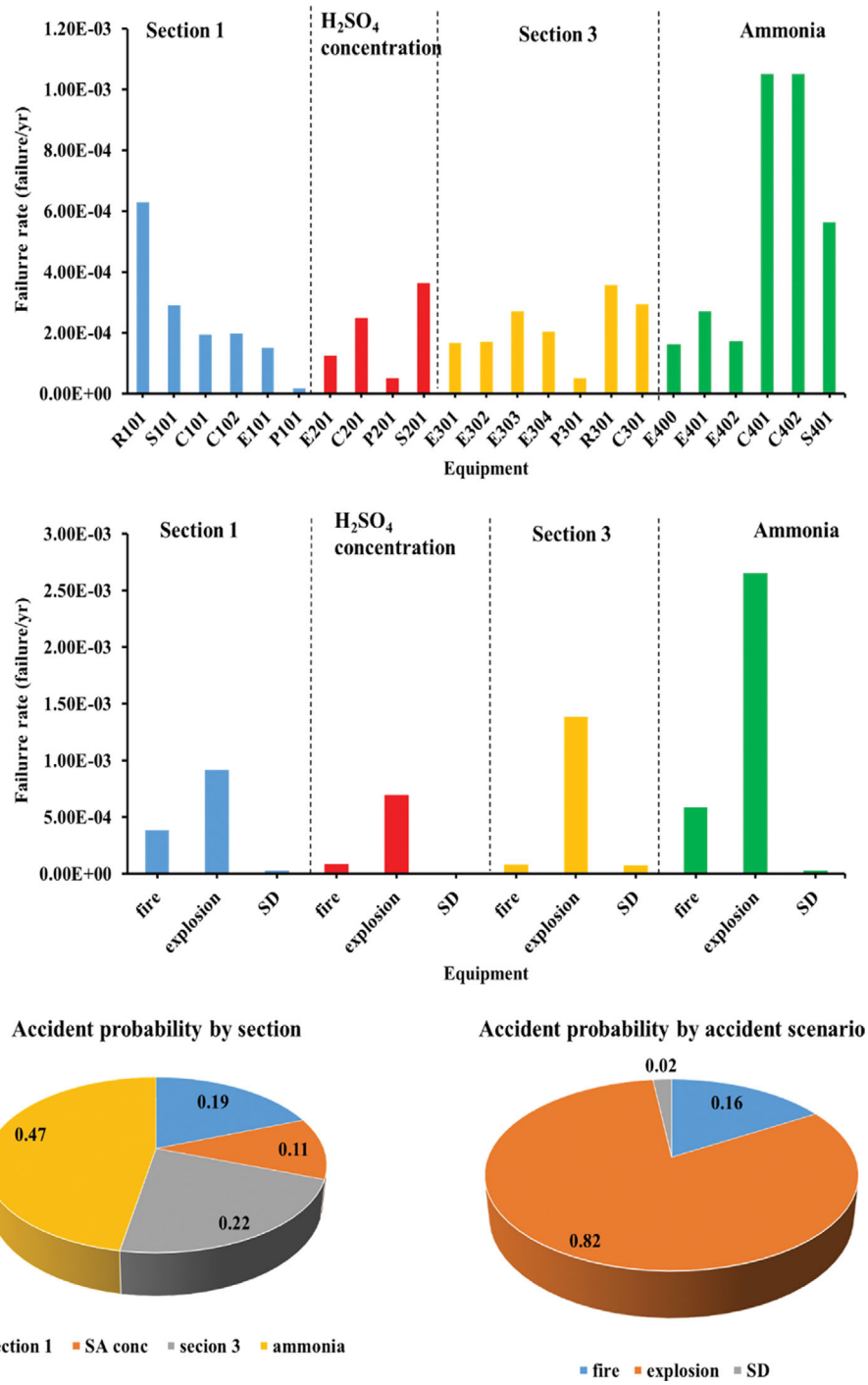

Fig. 8. The risk assessment on integrated ammonia production and modified sulfur iodine cycle.

failure rate. Explosion, fire, and structural damage contributed 82%, 16%, and 2% to the overall system in terms of accident scenarios.

4. Accident Injury Cost Calculation

The accident injury cost was evaluated for accident cure cost as represented in Fig. 9. The accident injury cost represents a quantitative measure of accident scenario to 200,000 nearby the facility. From an accident-based perspective, the accident cost contributed 84% and 16% of accident injury cost to the overall system, respectively. For the sectional based contribution, section 1 (Bunsen process), SA concentration, section 3, and ammonia production process contributed 45%, 29%, 19%, and 6% to the accident injury cost in the overall system, respectively.

The analysis shows that explosion from ammonia was the highest health injury cost since it involved hydrogen and high pressure causing a severe accident. That leads to serious injury with high compensation costs. Section 3, temperature with high temperature, contributes to the second largest portion since this process is involved in the high temperature. H_2SO_4 concentration section ex-

Table 4. The HAZOP identification of equipment type [30]

Equipment type	ID	Accident
Reactor	E101, E201, E301, E302, E304 E304, E400, E401, E402	Explosion Fire
Column	C101, C102, C201, C301, R301 (column reactor)	Explosion Fire Structure damage
Pump	P101, P201, P301	Explosion Structure damage
Vessel Drum	S101, S201, S401	Explosion Fire
Heat Exchanger	E101, E201, E301, E302, E303, E304, E400, E401, E402, E403	Explosion Fire
Compressor	C401, C402	Explosion Structure damage

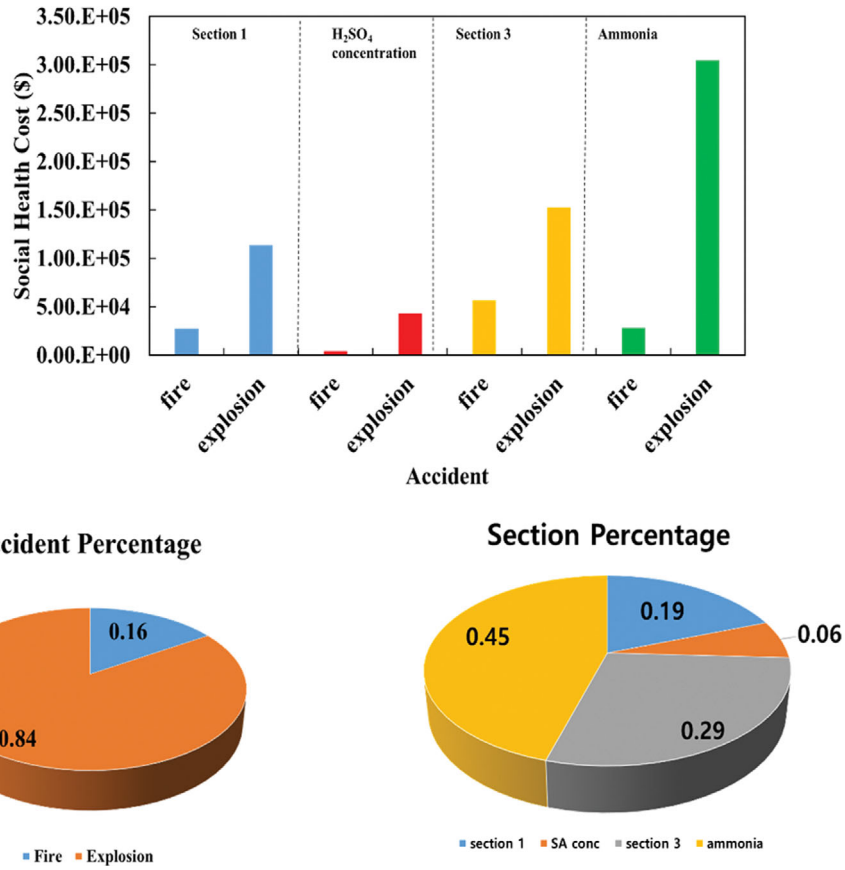

Fig. 9. Accident injury cost evaluation on integrated ammonia production and modified sulfur iodine cycle.

hibited the smallest health injury cost since it has the lowest flow rate. Section 1 exhibited the social cost values between H_2SO_4 concentration and section 3 since section 1 exhibited the similar flow rate and lower operating temperature and pressure compared to section 3.

This sequence proportion of accident injury cost agrees with the risk analysis that the explosion and ammonia process contributes the most to the health injury cost. In addition, SA conc, section 1, section 3, ammonia production contributed to the overall system in increasing order in both analyses.

5. Safety Investigation of Effect on Neighboring Section

The initial failure of the individual section on the neighboring section has been investigated as shown in Fig. 10. The red X mark indicates the section that accident was initiated. The blue X mark

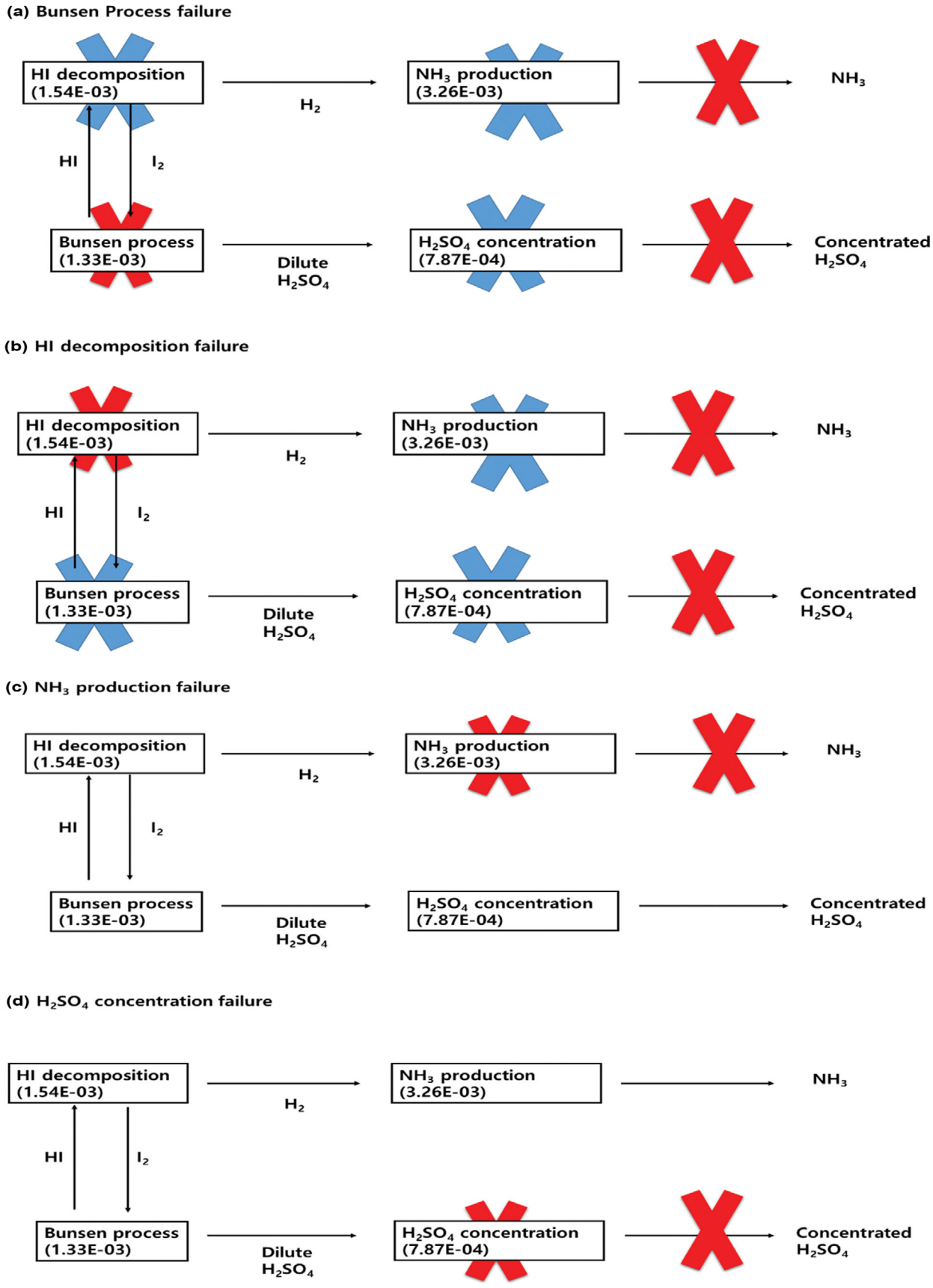

Fig. 10. Safety investigation of effect on neighboring section and partial failure rate. (a) Bunsen process failure, (b) HI production failure, (c) NH_3 production failure, (d) H_2SO_4 concentration failure.

Table 5. Summary table illustrates the consequence of failure initiation in each section. Total failure rate, the secondary failure section (sequential failure section after the initial failure), and available products are also demonstrated

Cases	Failure rate (failure/yr)	Secondary failure	Available product
(A) Bunsen process	6.92.E-03	HI decomposition NH_3 production H_2SO_4 concentration	None
(B) HI decomposition	6.92.E-03	HI decomposition NH_3 production H_2SO_4 concentration	None
(C) NH_3 production	3.26.E-03	None	Concentrated H_2SO_4 H_2
(D) H_2SO_4 concentration	7.87.E-04	None	NH_3 Diluted H_2SO_4

was sequential malfunctioned section as a result of initial event. Table 5 shows a summary of total failure rate, secondary (sequential) failure, and available production.

The initial failure in Bunsen section leads to failure in all the sections (Fig. 10(a)). This notion is because unavailability of H_2SO_4 production leads to failure in H_2SO_4 concentration to high grade, while unavailability of HI decomposition leads to failure in H_2 production with HI decomposition section. As a chain of event, failure in providing H_2 to NH_3 production section resulted in NH_3 production. The total failure rate was 6.92E-03 failure probability/year, and secondary failures were HI decomposition, H_2SO_4 concentration, and NH_3 production (Table 5). None of the products would be available.

The failure in HI decomposition section leads to the same result as Bunsen process failure case (Fig. 10(b)). If HI decomposition failed, Bunsen reaction would not occur since one of the reactants in Bunsen reaction, I_2, would not be provided to the Bunsen reactor. As a result, concentrated H_2SO_4 would not be produced. NH_3 would not be produced as a consequence of failure in H_2 production. The total failure rate was 6.92E-03 failure probability/year, and secondary failures were HI decomposition, H_2SO_4 concentration, and NH_3 production (Table 5). None of the products would be available.

The failure in NH_3 production would not affect other sections because this section was not interconnected to other sections (Fig. 10(c)). Therefore, failure in NH_3 production section would lead to no NH_3 produced. The total failure rate was 3.26E-03 failure probability/year, and secondary failure was NH_3 production (Table 5). Concentrated H_2SO_4 and H_2 would be available.

The failure in H_2SO_4 concentration section would not affect other sections because this section was not interconnected to other sections (Fig. 10(d)). Therefore, failure in H_2SO_4 concentration would lead to low concentration (diluted) H_2SO_4 concentration section. The total failure rate was 7.87E-04 failure probability/year, and secondary failure was NH_3 production (Table 5). Diluted H_2SO_4 and NH_3 would be available.

An additional streamline/safety system on HI decomposition and Bunsen reaction was suggested to be equipped since either of section leads to failure in all the sections with no products produced. Otherwise, failure in NH_3 production section produced at least H_2 and concentrated H_2SO_4 as selling products. Failure in H_2SO_4 only produced NH_3 as selling product. Diluted H_2SO_4 product was difficult to consider as selling product. The failure in H_2SO_4 concentration, NH_3 production, and Bunsen process and HI decomposition contributed to the higher failure rate in ascending order.

As a future study, the effect of failure initiation in individual equipment-based should be studied with sequential malfunctioning equipment as a realistic approach. Also, the effects of operation conditions on (1) NH_3 production (2) H_2SO_4 production should be considered to observe the best scenario and the worst scenario for parameter adjustment.

CONCLUSIONS

A novel integrated modified sulfur cycle and ammonia production process was suggested for the co-generation of sulfuric acid. Exergy analysis was implemented to investigate the thermodynamic feasibility and useful energy in each equipment. Heat integration and economic analysis were conducted to minimize the total cost of capital operating cost by searching the minimum heat transfer area. The FTA technique was implemented to analyze the failure probability in each equipment, accident type, and overall contribution. The risk assessment result was implemented in the accident injury cost analysis to investigate the cost corresponding to each accident scenario. The effect of failure in each section (partial) was investigated in terms of available products, failure rate, and secondary (consequential) failure. The following findings were extracted from this study.

(1) The exergy assessment confirmed that section 3 exhibited the lowest exergy efficiency and highest exergy destruction due to the largest temperature difference involved with a large flow rate. In terms of section, sulfuric acid concentration, section 1, ammonia production, and section 3 were contributed to 4%, 8%, 73%, and 15% to the overall system in exergy destruction. The heat exchanger, reactor, separator, turbine, pump contributed 75%, 14%, 11%, 4%, and 3% to the overall system for exergy destruction.

(2) The heat integration - economic assessment confirmed that the total cost was estimated to be reduced by 10.9% at the minimum temperature difference of 39 °C.

(3) The failure rate contribution to the overall system was 19%, 11%, 22%, and 47% from the Bunsen section, H_2SO_4 concentration section, HI decomposition section, ammonia production section explosion, fire, and structural damage contributed 82%, 16%, and 2% to the overall system in terms of accident scenario.

(4) The accident cost contributed 84% and 16% of accident injury cost to the overall system, respectively. For the sectional based contribution, section 1 (Bunsen process), SA concentration, section 3, and ammonia production process contributed 45%, 29%, 19%, and 6% to the accident injury cost in the overall system, respectively.

(5) Failure in Bunsen process and HI decomposition led to failure in production of all the products. Failure in NH_3 production

section led to production in concentrated H_2SO_4 and H_2. The failure in H_2SO_4 section led to production in NH_3 and diluted H_2SO_4 concentration. The failure in H_2SO_4 concentration, NH_3 production, and Bunsen process and HI decomposition contributed to the higher failure rate in ascending order.

This research was conducted to contribute to utilizing hydrogen energy and polygeneration processes to reduce the number of processes effectively. This investigation provides a guideline for the diagnosis of two integrated processes. For further study, a comparison between ammonia-modified cycle integration and conventional sulfuric acid process-Haber-Bosch-hydrogen production could be conducted for detailed comparison in terms of safety, economy, and heat. Furthermore, the effects of operation conditions on (1) NH_3 production (2) H_2SO_4 production should be determined to observe the best scenario and the worst scenario for parameter adjustment.

ACKNOWLEDGEMENT

This work was supported by the National Research Foundation of Korea (NRF) grant funded by the Korean government (MSIP: Ministry of Science, ICT and Future Planning) (No. NRF-2019 M2A7A1001811).

REFERENCES

1. M. A. Rosen, *Energy*, **35**, 1068 (2010).
2. A. A. Kiss, C. S. Bileda and J. Grievink, *Chem. Eng. J.*, **158**, 241 (2010).
3. M. Tejada-Iglesias, J. Szuba, R. Koniuch and L. Ricardez-Sandoval, *Ind. Eng. Chem. Res.*, **57**, 8253 (2018).
4. Grand View Research. Sulfuric Acid Market Size, Share & Trends Analysis Report by Raw Material (Element Sulfur, Base Metal Smelters, Pyrite Ore), By Application (Fertilizers, Chemical Manufacturing, Refinery, Textile), and Segment Forecasts, 2018-2025. GRV-2-68038-231-0; 2016.
5. Grand View Research. Ammonia Market Size, Share & Trends Analysis Report by Product Form (Liquid, Gas, Powder), by Application (Fertilizers, Textile, Pharmaceuticals, Refrigerants), by Region, and Segment Forecasts, 2018-2025. GRV-2-68038-207-5; 2017.
6. B. Lee, J. Park, H. Lee, M. Byun, C. W. Yoon and H. Lim, *Renew. Sustain. Energy Rev.*, **113**, 109262 (2019).
7. M. J. King, W. G. Davenport and M. S. Moats, Sulfuric Acid Manufacture Analysis, Control, and Optimization. Elsevier (2013).
8. O. Kirk, *Encyclopedia of chemical technology,* John Wiley & Sons (1984).
9. Y. Bicer, D. Iharahim, Z. Calin, V. Greg and R. Frank, *J. Clean. Prod.*, **135**, 1379 (2016).
10. Z. Hanfei, W. Ligang, V. Jan, M. Francois and D. Umberto, *Appl. Energy*, **208**, 195 (2017).
11. D. Orrego, S. Sharma, S. Oliveira Jr. and F. Marechal, *J. Clean. Prod.*, **44**, 118647 (2020).
12. S. Hwangbo, S. Lee and C. Yoo, *Appl. Energy*, **208**, 195 (2017).
13. L. Zhu, L. Li and J. Fan, *Chem. Eng. Res. Des.*, **104**, 792 (2015).
14. M. Mehrpooy and R. Habibi, *J. Clean. Prod.*, **275**, 12386 (2020).
15. J. H. Norman, G. E. Besenbruch, L. C. Brown, D. R. O'Keefe and C. L. Allen, Report, General Atomics Corp (1982).
16. L. C. Brown, G. E. Besenbruch, R. D. Lentsch, K. R. Shultz, J. F. Funk, P. S. Pickard, A. C. Marshall and S. K. Showalter, Report, General Atomics Corp (2020).
17. Y. K. Shin, K. Lee, Y. Kim, J. Chang, W. Cho and K. Bae, *Int. J. Hydrogen Energy*, **37**, 16604 (2012).
18. S. Kasahara, J. Iwatuski, H. Takegami, N. Tanaka, H. Noguchi, Y. Kamiji, K. Onuki and S. Kubo, *Int. J. Hydrogen Energy*, **42**, 13477 (2017).
19. D. G. Rodriguez, C. A. B. D. Lira, L. R. G. Parra, C. R. G. Hernandez and R. D. Valdes, *Energy*, **147**, 1165 (2018).
20. Z. Ping, W. Laijun, C. Songzhe and X. Jingming, *Renew. Sustain. Energy Rev.*, **81**, 1802 (2018).
21. J. Park, K. Nam, S. Heo, J. Lee, I. B. Lee and C. K. Yoo, *Korean Chem. Eng. Res.*, **58**, 235 (2020).
22. J. Park, S. Lee and I. Lee, *J. Chem. Eng. Jpn.*, **52**, 638 (2019).
23. A. Giaconia, G. Caputo, A. Ceroli, M. Diamanti, V. Barbossa, P. Tarquini and S. Sau, *Int. J. Hydrogen Energy*, **32**, 532 (2007).
24. B. J. Lee, H. C. No, H. J. Yoon, S. J. Kim and E. S. Kim, *Int. J. Hydrogen Energy*, **33**, 2200 (2008).
25. S. R. Sapute, J. Park and S. T. Revankar, *Adv. Chem. Eng. Res.*, **4**, 1 (2015).
26. M. Sakurai, H. Nakajima, K. Onuki and S. Shimizu, *Int. J. Hydrogen Energy*, **25**, 206 (2000).
27. J. E. Murphy and J. P. O'Connell, *Int. J. Hdyrogen Energy*, **37**, 4002 (2012).
28. V. Immanuel and A. Sakula, *Int. J. Hydrogen Energy*, **37**, 4829 (2012).
29. R. Liberatore, M. Lanchi, G. Caputo, C. Felici, A. Gianoia, S. Sau and P. Tarquini, *Int. J. Hydrgoen Energy*, **37**, 8939 (2012).
30. J. Park, P. Ifaei, A. H. Ba Alwai, U. Safder and C. K. Yoo, *Int. J. Hydrogen Energy*, **45**, 14578 (2020).
31. A. Rong and R. Lahdelma, *Renew. Sustain. Energy Rev.*, **53**, 363 (2016).
32. P. Ifaei, U. Safder and C. K. Yoo, *Energy Convers. Manage.*, **197**, 111851 (2019).
33. D. A. Crowl and J. F. Louvar, *Chemical process safety fundamentals and applications*, Prentice Hall, New York (2011).
34. P. Ifaei, J. Rashidi, and C. K. Yoo, *Energy Convers. Manage.*, **123**, 610 (2016).
35. I. Dincer and M. A. Rosen, Exergy: energy, environment and sustainable development, Newnes (2012).
36. S. Kim, J. Guo, K. I. Ahn and J. C. Lee, *American Nucl. Soc.*, **117**, 951 (2017).
37. J. E. Murphy and J. P. O'Connell, *Fluid Phase Equilia*, **288**, 99 (2010).
38. A. Tripodi, M. Compagoni, E. Bahadori and I. Rossetti, *J. Ind. Eng. Chem.*, **66**, 176 (2018).
39. N. R. Brown, S. Oh, S. T. Revankar, K. Vierow, S. Rodriguez, R. Cole Jr. and R. Gauntt, *Nucl. Technol.*, **167**, 95 (2009).
40. J. Rashidi and C. K. Yoo, *Energy*, **155**, 504 (2018).
41. S. Dehghani and H. Sayyaadi, *Int. J. Hydrogen Energy*, **38**, 9074 (2013).
42. F. Yilmaz and R. Selbas, *Energy*, **140**, 520 (2017).
43. R. Smith, *Chemical process design and integration*, John Wiley & Sons (2005).
44. S. Kim and J. C. Lee, *Annals of Nuclear Energy*, **139**, 107248 (2020).
45. R. Turton, R. C. Bailie, W. B. Whiting, J. A. Shaeiwitz and D. Bhat-

tacharyya, Pearson (2013).
46. Y. I. Kim, National Health Insurance Statistical Year book, NHIS (2018).
47. SINTEF Industrial Management, Offshore Reliability Data Handbook, Norway (2002).
48. M. Shariff, A. M. Shariff, A. Buang, M. S. Shaikh and M. I. Khan, *Chem. Eng. Technol.*, **42**, 524 (2019).
49. S. Mannan, Lees' loss prevention in the process industries: hazard identification, assessment, and control, Elsevier (2012).